Master Thesis

Calibrating Courier/Overhead Manipulator Pairs in Minifactory

Rob Schlender

Advisors

Dr. Ralph Hollis & Dr. Alfred Rizzi

Robotics Institute
School of Computer Science
Carnegie Mellon University, Pittsburgh PA

2005

Contents

List of Tables

List of Figures

1 Introduction

1.1 Motivation for Minifactory

Demands placed on manufacturing companies are changing as the number of precise, complex, electro-mechanical devices required in today's society rapidly increases. Many of these products must be assembled very accurately, but have short product lifecycles. Producing products with these demands requires the manufacturing process to blend agility with accuracy. Current assembly lines are inadequate to meet these requirements. They take months to set-up, are hard to modify once assembled, and are often insufficiently accurate. With the large premium placed on being "first to market" and with rapidly changing marketplace requirements making easy product modifiability essential, we are in need of new manufacturing techniques.

The Architecture for Agile Assembly (AAA) is a response to this need. The AAA consists of agent-based robotic elements that are precise, modular, and extensible [1]. Each agent consists of mechanical components and a powerful computer; also, the agents are aware of their own capabilities and the capabilities of other agents in the factory. Importantly, these AAA factories can be set up in a matter of days or weeks because AAA agents are designed to have common mechanical, communicative, and algorithmic interfaces.[1].

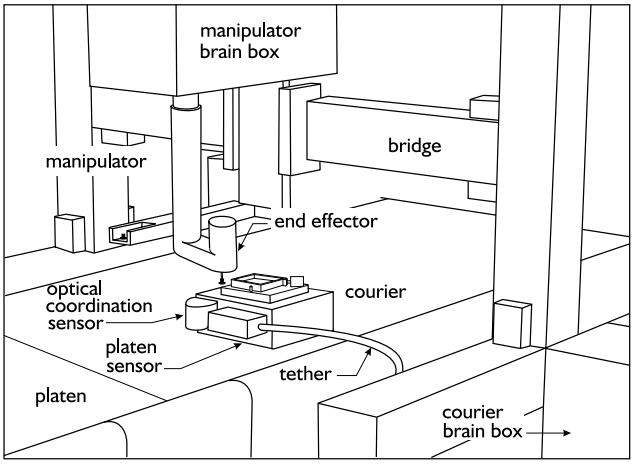

Figure 1: A portion of the minifactory showing a courier and OHM

Minifactory, which is being constructed in the Microdynamic Systems Laboratory (MSL) at Carnegie Mellon University, is an example of a AAA factory. Minifactory consists of two types of agents: overhead processors and couriers (see Fig. 1). Courier robots move precisely

along a table-top platen while carrying sub-assemblies on their back. To manufacture products, couriers move under overhead processors. Once there, overhead processors and couriers cooperate to perform precision assembly tasks. Overhead manipulators (OHM), a subset of overhead processors, are used to manipulate parts on a courier. OHM's have 2 degrees of freedom (z and θ), while couriers have 3 degrees of freedom(x, y and limited θ). These low degree-of-freedom robots work in a cooperative fashion to precisely assemble complex electro-mechanical products.

1.2 The Need for Calibration

To meet today's manufacturing demands, minifactory is designed for rapid deployment and quick modification. OHM's and couriers are attached to the factory by hand. OHM's clamp to adjustable bridges mounted above the factory's platen. Couriers are then placed on the factory's platen. This simple assembly allows the factory to be physically assembled and disassembled by unskilled persons in a matter of hours to days. However, this assembly results in couriers and OHM's being imprecisely positioned relative to one another. In order to precisely manufacture parts, they *must* be able to accurately and precisely position their end effectors relative to each other.

Several solutions to this problem exist. Teaching pendants can be used, but teaching a robot where to move can be an expensive and time consuming operation [2]. Using computer vision, the end effectors can servo to the proper relative pose(position and orientation). However, this requires special image processing hardware and specific vision algorithms have to be developed for each assembly task. Both of these solutions also require all the necessary physical hardware to be assembled before the teaching pendants or computer vision algorithms can be fully developed.

Another solution is to recover the kinematics of the OHM/courier pair. Using this approach, it's possible to program and simulate the entire factory in advance, without requiring all the necessary physical hardware to be assembled. Once the calibration procedure recovers the kinematics of the real factory, the simulated programs can be automatically compensated to work in the real factory. This is particularly appealing when rapid deployment is a priority.

There are also disadvantages to calibrating the kinematics of the courier/OHM pair. The calibration process requires special calibration hardware. Furthermore, recovering the kinematics usually requires a model of the robot. This robot model may not match the real robot very well. Fortunately, in minifactory the agents are precisely constructed and have

short kinematic chains. Therefore the model of the robots should fairly accurately represent the real system.

This report will focus on recovering the transform between a fixed frame on the courier and a fixed frame on the OHM. Using this transform one can recover the courier and OHM's relative pose. The transform between these fixed frames is unknown because of the simple and rapid assembly of the minifactory.

A manual calibration procedure could be developed to measure this transform. However, this would be in opposition to AAA goals, which require a factory to be easily assembled and modified. Furthermore, manual measurements are time consuming and require trained professionals. Instead, an automated calibration procedure will be developed using onboard sensors specifically designed to aid in this task.

This automated calibration procedure has several advantages over a manual approach. Depending on the task, it makes sense to calibrate courier/OHM pairs frequently (every hour or day) to ensure the best accuracy possible. Manually doing this would be time and labor intensive. Furthermore, if an agent needs to be replaced due to a breakdown, a spare can be quickly brought online, without a trained factory calibration specialist on hand. Finally, the resulting accuracy is not based on the skill of the professional making the measurements, but instead on the calibration procedure itself and the quality of sensors involved.

1.3 Calibration Overview

In the broadest sense, calibration is the process of using known measurements to determine the value of parameters which are infeasible to directly obtain. In minifactory, the optical coordination sensor's (OCS) measurements are used to determine the relative pose between the courier and OHM. The OCS is attached to the side of the courier. It functions by detecting light emitted from an LED mounted in the OHM.

The relative pose between the courier and OHM is recovered by creating a model that predicts the OCS output. This model contains two types of inputs: *variables* and *unknown parameters*. *Variables* are inputs with changing, but known values, such as actuator joint positions. *Unknown parameters* are inputs with constant, but unknown values. An example of an *unknown parameter* is the transform between a fixed frame on the courier and a fixed frame on the OHM. Determining the value of these *unknown parameters* is the goal of the calibration procedure.

The calibration procedure recovers the *unknown parameters* in a two step process. First,

the courier and OHM move to many different configurations. At each of these configurations the actuated joint positions are automatically recorded along with the OCS measurement. These actuated joint positions are the *variable* inputs into the model. Next, an initial guess is made for the *unknown parameters*. The recorded OCS output is compared against the model predicted OCS output for every collected measurement. The *unknown parameters* are adapted using the differences between the predicted and recorded sensor readings. This process of adapting the *unknown parameters* continues until the difference between the predicted and recorded sensor readings falls below a tolerance threshold. At this point the *unknown parameters* input into the model are assumed to be the *unknown parameters* in the real system. A more detailed explanation and justification of this procedure is provided in sections 3 and 4.

This report divides the calibration process into three parts:

1. Understand the courier and OHM components.
2. Build a model representing the courier/OHM pair.
3. Derive a calibration procedure to recover the parameters.

1.4 Scope of this Calibration Procedure

The calibration procedure *does not* directly recover the relative pose between the OHM's working end effector (eg. gripper, vacuum pickup) and the courier work surface. The calibration procedure only allows one to know the relative pose between a coordinate frame attached to the OHM's LED and a coordinate frame attached to the OCS.

In addition, there is no way to directly sense these working end effectors using the OCS, and therefore no way of directly recovering the relative pose between them. Instead, measurements relating the LED to the OHM's working end effector (eg. gripper, vacuum pickup) must be known. Measurements relating the position sensing detector (PSD), located in the OCS to the courier work surface also must be known. It's expected that these measurements will be made by the courier and OHM manufacturer. The measurements will be included in the agents profile, so there is no need to make manual measurements during the factory assembly. Suggestions on how courier and OHM manufacturers might make these measurements are included in the future work section.

2 Physical Components

A detailed description of the courier and OHM's role in the minifactory, as well as the capabilities relevant to calibrating the pair, is presented so as to provide insights into the model's construction.

2.1 Courier

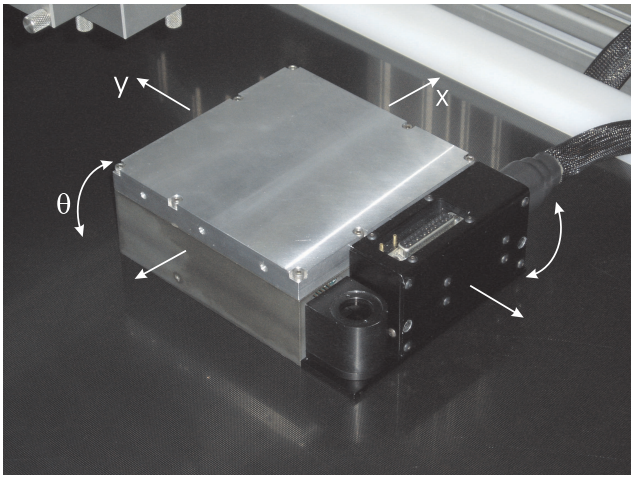

Figure 2: A courier and its degrees of freedom.

Couriers play several roles in the factory. They move sub-assemblies through the factory from one overhead processor to another. In this role, they replace the traditional factory's conveyor belt. Their high precision, rapid movement also lets them work in a cooperative fashion with overhead processors during assembly tasks. Furthermore, couriers can act as mobile parts feeders.

Couriers are based on linear stepper motors and use Sawyer motor technology [3]. They fly 10-15 microns above the platen, on an air bearing. The platen is an ultra-flat steel surface with a two-dimensional waffle-iron pattern of teeth [4]. The gaps between the teeth are filled with epoxy to provide a smooth bearing surface [4]. Orthogonal linear motors in the courier use the platen, surface to maneuver the courier.

The linear motors and platen surface give couriers 3 degrees of freedom: x, y translation and limited θ rotation (Fig. 2). Couriers travel up to 1.5 m/s[4]. The translation range of the courier is limited only by the size of the platen surface, and the tether connecting the courier to it's external computing,power, and air supply. The θ rotation of the courier is limited to

$\pm 2°$.

A magnetic AC platen sensor was designed at Carnegie Mellon University. This sensor is installed in the center of the bottom courier surface. Using this sensor, the courier has an x, y position resolution of 200 nm(1σ) [5]. In addition, this sensor gives the courier a θ rotation resolution of .0014 ° [5].

2.2 Overhead Manipulator

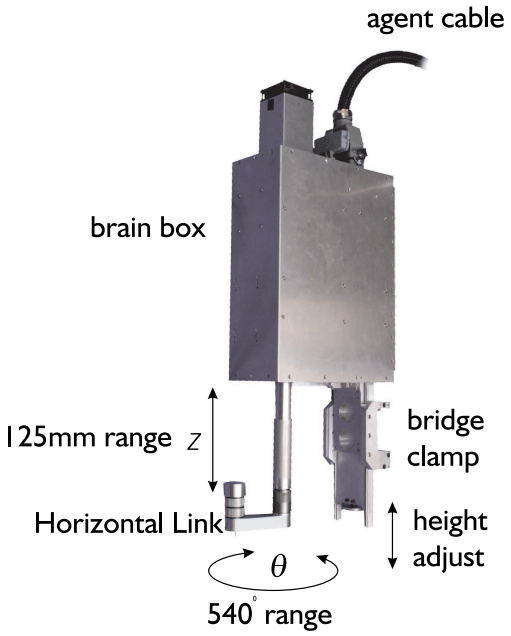

Figure 3: An overhead manipulator

OHM's also play several roles in the factory. Their primary role is to pick up a part from a parts feeder, and place the part on the courier. OHM's can also be used to transfer sub assemblies from one courier to another. Along with the courier, they replace the traditional factory's SCARA robot.

OHM's have actuated z translational and θ rotational movement about a coincident axis (Fig. 3). The z actuators have a range of 125 mm with a resolution of 2 µm. OHM's also have a 540 ° θ range of movement with a resolution of .0005 °.

To aid in the calibration process, LED beacons are installed in the horizontal link of the OHM. The light emitted from the LED is detected by the OCS.

2.3 Optical Coordination Sensor

The OCS is mounted to the side of the courier and used to detect LED's mounted in the OHM's horizontal link. The primary purpose of this sensor is to aid in calibrating the courier/OHM pair. The field of view of the OCS was measured, and shown to be at least 76 deg [6] (Fig. 4).

A lens is installed in the OCS in order to increase the amount of light collected from the LED. This lens is coated with anti-reflective material to minimize reflections.

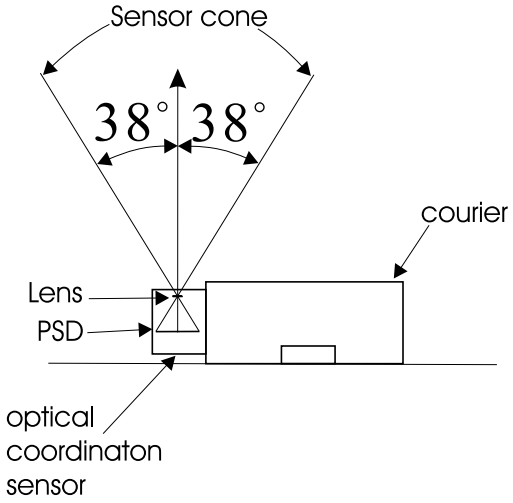

Figure 4: The OCS field of view.

The OCS contains a duo-lateral position sensing detector (PSD). This PSD senses the centroid position of the light spot shining on it's surface [7]. The resolution of the centroid position on the PSD was measured to be 150 nm (1 σ) [7] along each axis.

3 Mathematical Model

An accurate model of how the OHM/courier pair affect the OCS output is now described. This model returns a 2x1 vector, containing the expected x, y light spot position from the OCS. To build this model, the courier, OHM, and OCS are analyzed to determine how they affect the OCS output. Models of how each of these components affect the OCS output are then constructed. Additionally, the uncertainties relating these individual components are modeled. At the end of this section, the models are combined into a complete courier/OHM model that predicts the expected OCS output.

These models have two types of inputs: *variables* and *parameters*. As explained in section 1.3, *variables* are inputs with known, changing values, while *parameters* are inputs with constant, unknown values.

To calculate the expected OCS output, the relationship between the LED's position and the OCS components must be found. The relative position of the OCS and LED changes depending on the movement of the courier and OHM. This movement can be modeled by describing the courier and OHM's degrees of freedoms as kinematic chains. The Denavit-Hartenberg (DH) convention is then used to represent these kinematic chains [8].

3.1 Courier Model

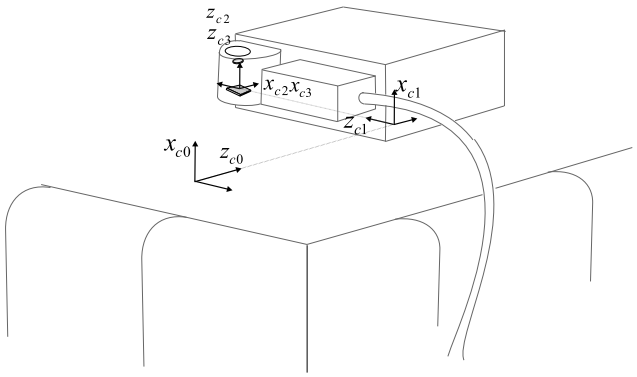

Figure 5: The coordinate frames of the courier

In this section, the effect of the courier's movement on the OCS components is modeled. This is accomplished by fixing a frame, $c0$, somewhere in space, and attaching a frame, $c3$, to the OCS. The courier's degrees of freedom (x, y translational and θ rotational) are modeled as a Prismatic-Prismatic-Revolute (PPR) mechanism. The $c3$ frame is defined to be at the

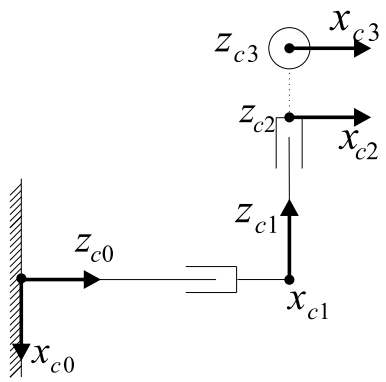

Figure 6: A kinematic representation of a courier.

electrical center of the PSD surface. Additionally, this frame is oriented with the actuated x and y directions of the courier.The $c0$ frame is defined such that, when all of the actuated joints of the PPR mechanism are 0, the frames $c0$ and $c3$ share the same origin.

DH parameters for the courier are shown in Table 1.

Link No.	a_i	α_i	d_i	θ_i
1	0	$\frac{\Pi}{2}$	cd_1	0
2	0	$\frac{\Pi}{2}$	cd_2	$\frac{\Pi}{2}$
3	0	0	0	ct_3

Table 1: DH parameters for the courier

The cd_1 and cd_2 variables control the relative position of the courier from the base frame while ct_3 is the current rotation of the courier about the electrical center of the PSD.

Converting the DH parameters shown in Table 1 into their equivalent transformations yields three 4x4 matrices: T_{c1}^{c0}, T_{c2}^{c1}, and T_{c3}^{c2} where T_i^j denotes the transform of frame i with respect to frame j.

The transform of frame $c3$ with respect to $c0$ is shown in equation 3.1.

$$T_{c3}^{c0} = T_{c1}^{c0} \cdot T_{c2}^{c1} \cdot T_{c3}^{c2} \tag{3.1}$$

This section a model was constructed to describe the effect of the courier's movement on the OCS. Three variables (cd_1, cd_2 and ct_3) and no parameters were defined as inputs into this model.

3.2 Overhead Manipulator Model

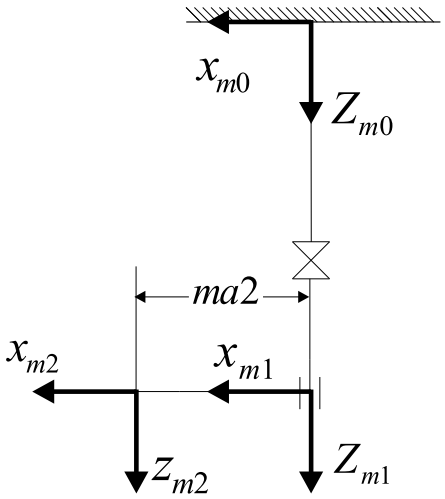

Figure 7: A kinematic representation of the OHM

In this section, the effect of the OHM's movements on the LED pose is modeled. This is done by fixing a frame $m0$ somewhere in space and attaching a frame, $m2$, to the LED (Fig. 7). The OHM's degrees of freedom (z translational and θ rotational) are modeled as a Revolute-Prismatic (RP) mechanism.

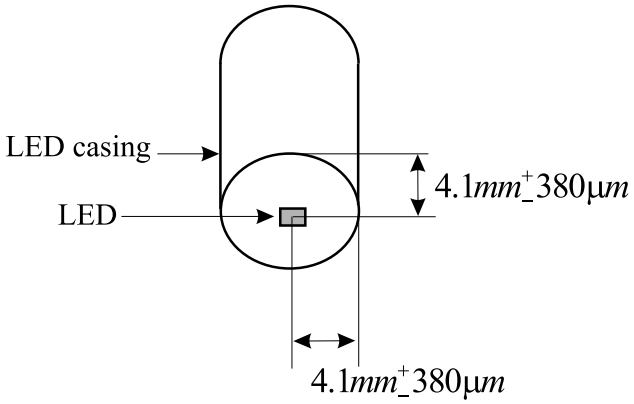

Figure 8: The tolerance of the diode mounted in the LED case

Precisely defining the $m2$ frame at the LED requires some consideration because the light emitting diode is not precisely placed inside the LED case. Based on correspondence with the manufacturer, the diode installed in the LED case has an x, y tolerance of $\pm 380um$ (Fig. 8). The position of the diode is important because the calibration procedure recovers the

position of the light source. The $m2$ frame is attached to the center of this light emitting source. For the remainder of this report, LED refers to the light emitting source, unless otherwise specified.

Knowing the actuated joint values of the OHM and the perpendicular distance the LED is from the rotational axis is sufficient to model how OHM movements change the LED position. Due to the LED tolerance, an unknown parameter, $ma2$ is added to the model, which represents the distance the light emitting emitting source is from the OHM's θ axis (Fig. 7).

The $m0$ frame is defined such that, when all of the actuated joints of the RP mechanism are 0, the frames $c0$ and $c3$ have the same orientation, and are only separated by a constant translation $ma2$ along the $m0_x$ axis (Fig. 7).

Link	a_i	α_i	d_i	θ_i
1	0	0	0	$mt1$
2	$ma2$	0	$md2$	pi/2

Table 2: DH parameters for the overhead manipulators

Table 2 shows the DH parameters for the RP mechanism. $mt1$ is the current angle of the OHM, while $md2$ is the current extension of the prismatic joint of the OHM.

The DH parameters shown in Table 2 are used to generate the following transformation matrices: T_{m1}^{m0}, T_{m2}^{m1}.

Now, we can transform the LED to the overhead manipulator's base frame (m0) using Equation 3.2 because the end effector's origin is defined to be at the LED.

$$T_{m2}^{m0} = T_{m1}^{m0} \cdot T_{m2}^{m1} \cdot [\ 0 \quad 0 \quad 0 \quad 1\ ]^T \tag{3.2}$$

To summarize, a model of the effect of the OHM's movement on a frame attached to the LED, relative to the fixed $m0$ frame was constructed. Two *variables* (md_1, and mt_2) which represent the OHM's z and θ actuated values were defined. An unknown parameter $ma2$ was defined that represents the radius from the OHM's axis of rotation to the LED.

3.3 Relating the overhead manipulator to the courier

A way of relating the courier and OHM models is described next. Remember, the OHM is clamped inaccurately to the adjustable bridge above the platen. The uncertainty between the

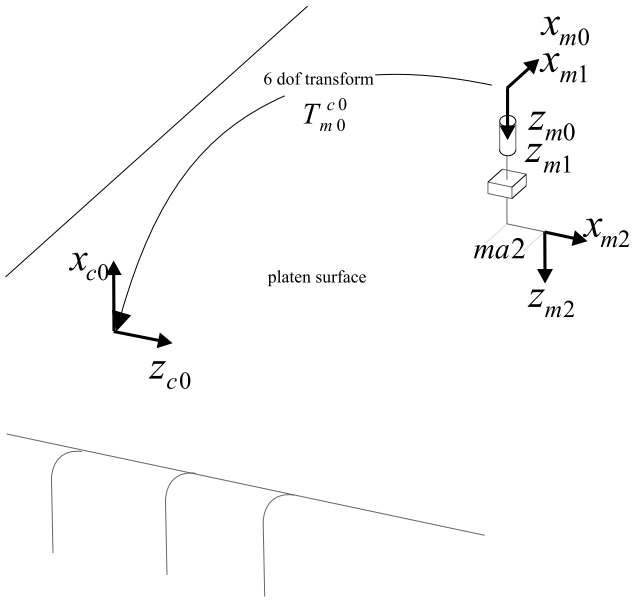

Figure 9: The transform T_{m0}^{c0} between the courier and OHM base frames

courier and the OHM is modeled using a 6 DOF transform, called T_{m0}^{c0}. This transform exists between the OHM and courier base frames (Fig. 9). Note, since the base frames are fixed, this transform is constant. The rotational portion of this transform is parameterized using the Euler angle convention: ZYX starting from the $c0$ coordinate frame. γ is the rotation about z, ψ is the rotation about Y, and ϕ is the rotation about X.

As mentioned in the introduction, this transform is the *primary* uncertainty in relating courier and OHM. Recovering the parameters that make up T_{c0}^{m0} is the focus of this calibration procedure. This transform introduces 6 new parameters into the model. γ,ψ, and ϕ are the unknown rotations between the base frames, whereas x_b, y_b, and z_b, are the translations between the $c0$ frame with respect to $m0$.

3.4 Optical Coordination Sensor Model

The OCS is used to detect light from the LED. It has three primary components that affect the reported light spot position: the amplifier electronics, the lens, and the PSD.

The PSD outputs 2 currents for each axis (Fig. 11). In order to determine the centroid position, these currents are amplified. Differences in these amplifier gains cause errors in the predicted position of the light spot. To mitigate this problem, highly accurate analog circuits were designed to account for such variations [6]. Therefore, the amplifiers are not modeled.

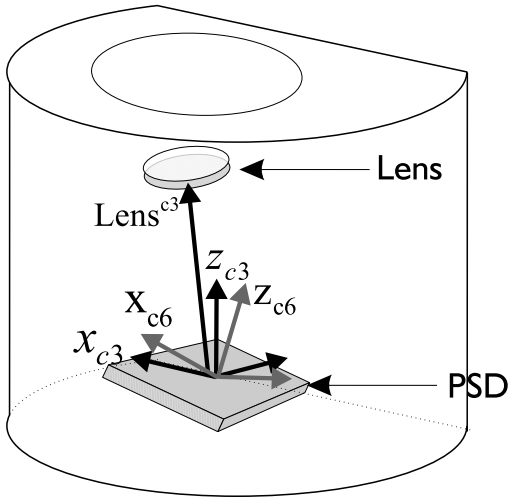

Figure 10: A close-in view of the OCS showing the PSD and Lens

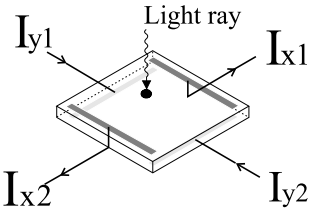

Figure 11: PSD sensor

A lens in the OCS is used to collect light from the LED in the OHM. The position of the lens is estimated from manufacturing tolerances to vary by $\pm 100\mu m$ along each axis relative to the PSD. This variation affects where the light hits the PSD. Additionally, any real lens causes distortions. Parameterizing these distortions introduces many new parameters. However, since the PSD gives the "centroid of power density" for a light spot, the distortions caused by the lens can be ignored and the lens is modeled as a pinhole. The unknown position of the pinhole, is defined as a vector, $Lens^{c3}$, (Fig.10) from the couriers end effector frame ($c3$). This introduces three new *parameters*: $Lens_x^{c3}$, $Lens_y^{c3}$, and $Lens_z^{c3}$.

Installing the PSD in the OCS housing results in another source of uncertainty. There is thought to be a $\pm 0.5^\circ$ rotational tolerance about each axis of the PSD and a $\pm 100\mu m$ tolerance in the x, y and z position. These tolerances affect where light hits the PSD surface, and consequently affects the output of the OCS.

The effect of the orientation of the PSD on the OCS output is modeled by attaching a frame, $c6$, to the PSD surface and relating it to the courier's end effector frame, $c3$. Since the PSD produces an x, y location of the light spot hitting it's surface it is reasonable to

define the $c6$ frame relative to this. The $c6$ x and y axes are defined to be identical to the x and y axes of the PSD. The $c6$ z axis is defined to be normal to the PSD surface. Using this definition for the $c6$ frame means the OCS outputs the centroid position of the light spot in $c6$ coordinates.

In order to associate the OCS output to the rest of the system, we relate the $c6$ frame and the courier end effector frame ($c3$) (Fig. 10). The $c3$ frame and $c6$ frame share the same origin because they are both defined to be on the PSD surface at the electrical-center. However, due to manufacturing tolerances the orientation of the PSD is unknown. We model the unknown orientation between the courier's end effector frame and $c6$ frame as a spherical wrist (Fig. 12). The DH parameters for the spherical wrist are shown in Table 3.

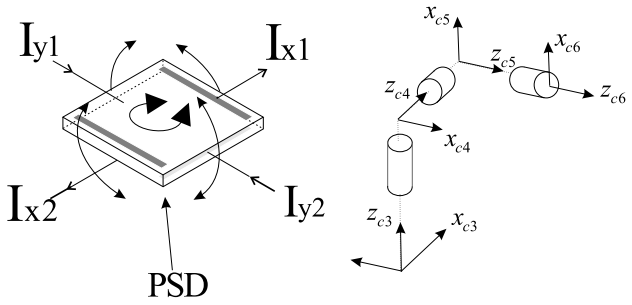

Figure 12: The spherical wrist between the courier end effector and PSD

Link No.	a_i	α_i	d_i	θ
4	0	$-\frac{\Pi}{2}$	0	ct_4
5	0	$\frac{\Pi}{2}$	0	ct_5
6	0	0	0	ct_6

Table 3: DH parameters for the optical coordination sensor

The ct_4, ct_5, and ct_6 are *parameters* that represent the joint angles of the spherical wrist. ct_4 also models the unknown rotation of the OCS in the courier side wall plane (Fig. 13). Converting the DH parameters from Table 3 into their equivalent transformations yields three 4x4 matrices: T_{c4}^{c3}, T_{c5}^{c4}, and T_{c6}^{c5}.

Coordinate frames $c3$ and $c6$ are related by the transformation in Equation 3.3.

$$T_{c6}^{c3} = T_{c4}^{c3} \cdot T_{c5}^{c4} \cdot T_{c6}^{c5} \tag{3.3}$$

Using Equations 3.1 and 3.3 the $c6$ frame is related to the courier base frame ($c0$).

$$T_{c6}^{c0} = T_{c3}^{c0} \cdot T_{c6}^{c3} \tag{3.4}$$

This transform will be useful later when all component models are combined to determine the expected OCS output.

The careful reader will notice that there are no parameters for the position tolerance of the PSD. This tolerance is included in the model, it is just that the position uncertainties are redundant with other parameters in the system. For our purposes, we care about accurately recovering the relative pose between the courier's OCS components and the OHM's LED. It makes no difference in the relative pose of the LED and PSD if the $c3$ frame is moved up 100um, or instead if the OHM's $m0$ frame is moved down 100um. The relative position between the PSD and the LED remain the same. The courier and OCS frames are carefully defined to remove these redundant parameters. Including the redundant parameters makes it harder to recover the parameters later in the identification step.

In the case of the PSD tolerances, the position tolerances are redundant with the T_{c0}^{m0} transform and $lens$ vector. This is because the end effector of the courier ($c3$) is carefully defined to be at the electrical center of the PSD surface. The frames $c0$, $c1$, and $c2$ are also defined relative to the PSD location. If the PSD moves up, so does frame $c3$ and therefore $c0$. If $c0$ moves up, the unknown translation parameters in the T_{c0}^{m0} transform change by the same amount. Defining the frames in this fashion "moves" the uncertainties to the T_{c0}^{m0} transform. Additionally, since the lens remained fixed in this scenario, the $Lens^{c3}$ vector can change to so it still points at the lens.

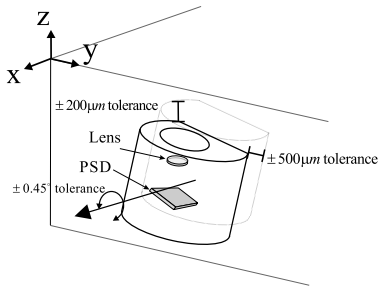

Figure 13: Optical coordination sensor mounting tolerance on a courier

Installing the OCS on the courier side wall results in a source of uncertainty because it's not mounted perfectly. Measurements revealed that the OCS is mounted with a rotational

tolerance of $\pm 0.45^\circ$ in the plane of the courier side wall (Fig. 13). These measurements also revealed the OCS is mounted with a y and z positioning tolerance of $\pm 500\mu m$ and $\pm 200\mu m$ respectively.

Again, these parameters are redundant with other parameters in the system. The position tolerances of the OCS are redundant with the translations parameters in the T_{c0}^{m0} transform. Furthermore, the rotational tolerance of the OCS, is redundant with the ct_4 unknown parameter in the orientation of the PSD.

The redundant uncertainties add to the total tolerance range the translation parameters that define the T_{c0}^{m0} transform. The frames Defining the frames ($c0$, $c1$, and $c2$) relative to the PSD "moves" the unknown to the T_{c0}^{m0} transform.

To summarize, a model of how the OCS affects the reported spot position was described and constructed. The effects on the light spot from the pose of the OCS, PSD, and position of the lens were modeled. Unmodeled effects include lens distortion and amplifier gain differences. This model also ignores small effects in the OCS, including ghosting from refractions in the lens, refractions from the absorption filter, and any optical axis misalignment with the PSD.

This model introduces several new *parameters*. $Lens_x^{c3}$, $Lens_y^{c3}$, and $Lens_z^{c3}$ are added because the pinhole representing the lens is unknown. ct_4, ct_5, and ct_6 are added to represent the orientation between the courier end effector frame and the PSD frame. The model of the PSD plane and lens do not have any *variables*.

3.5 Expected Optical Coordination Sensor Output

Models for the courier, OCS, and OHM, as well as a transform relating the base frames of the OHM and courier were constructed. Now the component models are combined to calculate the expected OCS output.

The light ray emitted by the LED that is sensed by the PSD, must travel through the pinhole. To determine where this ray hits the PSD, we transform the LED, PSD, and pinhole camera into the same frame.

Additionally, where the ray intersects the x, y plane of the $c6$ frame is also where it hits the PSD. Remember, this is because the $c6$ frame is defined to have the same pose as the PSD. We transform the LED, PSD, and pinhole camera into the $c6$ frame in order to easily use this restriction. These two constraints are sufficient to determine the expected OCS's output.

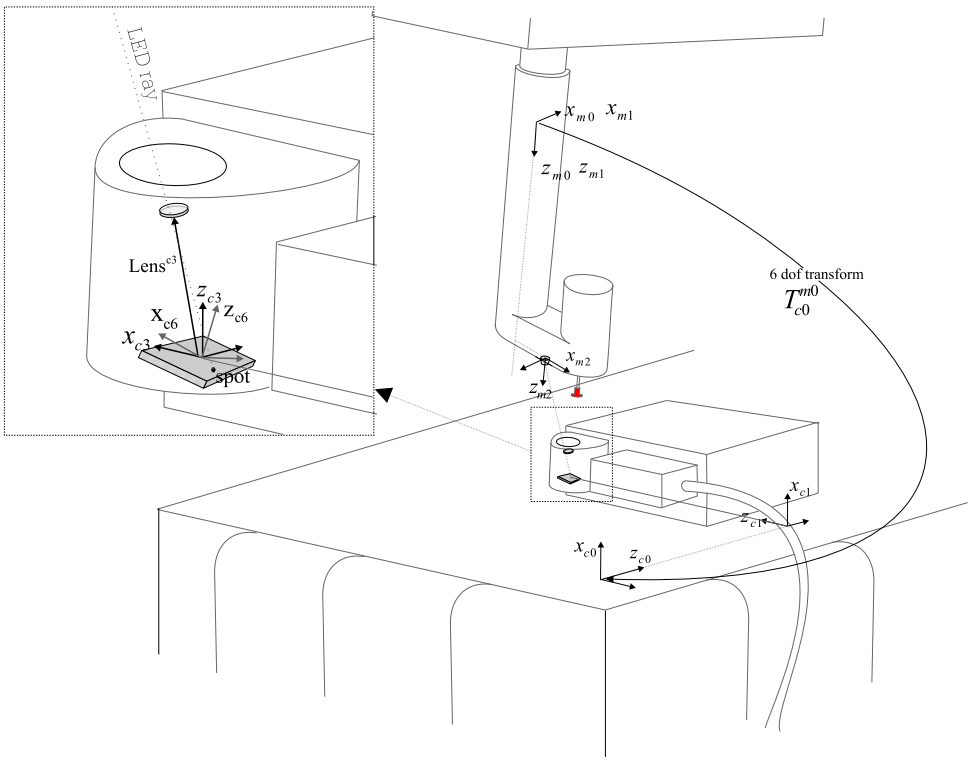

Figure 14: This shows all of the relevant coordinate frames and transforms.

First, the LED is transformed into the couriers base frame using Equations 3.2 and the transform T_{m0}^{c0}

$$LED^{c0} = T_{m0}^{c0} \cdot T_{m2}^{m0} \cdot [\ 0 \quad 0 \quad 0 \quad 1\ ]^T \tag{3.5}$$

The LED is transformed into the $c6$ frame using the inverse of the transform defined in Equation 3.4.

$$LED^{c6} = inv(T_{c6}^{c0}) \cdot LED^{c0} \tag{3.6}$$

Next, we transform the pinhole location into the $c6$ frame using the inverse of the transform in Equation 3.3.

$$Lens^{c6} = inv(T_{c6}^{c3}) \cdot Lens^{c3} \tag{3.7}$$

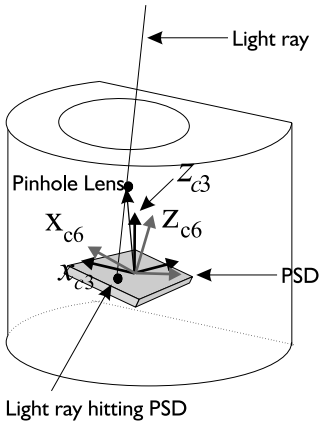

Figure 15: This shows how the ray that intersects the PSD travels in a line through the pinhole camera.

Now we have the PSD, pinhole camera, and the LED in the $c6$ frame. We represent the line (light ray) that hits the PSD using a parametric representation of a line.

$$x = s \cdot LED_x^{c6} + (1 - s) \cdot Lens_x^{c6} \tag{3.8}$$

$$y = s \cdot LED_y^{c6} + (1 - s) \cdot Lens_y^{c6} \tag{3.9}$$

$$z = s \cdot LED_z^{c6} + (1 - s) \cdot Lens_z^{c6} \tag{3.10}$$

As mentioned earlier we know that the line represented in the $c6$ frame intersects the PSD surface when z equals 0. Solving for s when $z = 0$ yields:

$$s = \frac{pinHole_z^{c6}}{pinHole_z^{c6} - LED_z^{c6}}$$

Finally, substituting s into equations 3.8 and 3.9 gives us the x and y values we expect from the sensor given this courier/OHM configuration.

To summarize, the *variables* input into the model that predicts the OCS output are shown in table 4 and *parameters* input into the model are shown in table 5. Remember, *variables* are inputs with changing, but known values; whereas *parameters* are inputs with constant

value that we find using the calibration procedure.

Variables	Description	tolerance
d_{c1}	distance courier moved from the c0 frame in the z_{c0} direction (mm).	$200nm$
d_{c2}	distance courier moved from the c0 frame in the $-x_{c0}$ direction(mm).	$200nm$
$ct3$	rotation of courier about z_{c3} (degrees)	0.0014°
d_m1	The extension of the OHM prismatic joint (mm)	$2\mu m$
$mt2$	The rotation of the OHM revolute joint (degrees)	$.0005^\circ$

Table 4: Variables in the model.

Unk Params	Tolerance	Description
$T^{c0}_{m0,x}$	$\pm 5mm$	
$T^{c0}_{m0,y}$	$\pm 5mm$	
$T^{c0}_{m0,z}$	$\pm 5mm$	Elements of the transform
$T^{c0}_{m0,\theta}$	$\pm 1^\circ$	relating the fixed courier
$T^{c0}_{m0,\psi}$	$\pm 1^\circ$	and OHM base frames
$T^{c0}_{m0,\phi}$	$\pm 1^\circ$	
$ma2$	$\pm 380\mu m$	distance LED is from axis-of-rotation of OHM.
$ct4$	$\pm 0.5^\circ$	The first rotation in the T^{c3}_{c6} transform
$ct5$	$\pm(0.5^\circ + .45^\circ)$	The second rotation of the T^{c3}_{c6} transform
$ct6$	$\pm 0.5^\circ$	The third rotation of the T^{c3}_{c6} transform
$Lens^{c3}_x$	$\pm 100\mu m$	x component of the vector to the center of the lens
$Lens^{c3}_x$	$\pm 100\mu m$	x component of the vector to the center of the lens
$Lens^{c3}_x$	$\pm 100\mu m$	x component of the vector to the center of the lens

Table 5: The parameters in the system we need to recover.

4 Calibration Procedure

Now that a model of the expected courier/OHM pair exists, the next step is to collect a useful set of measurements, and fit the unknown model parameters to the collected measurements.

The calibration procedure is broken into two parts:

- Measurement collection
- Fitting the unknown model parameters to the collected measurements.

4.1 Measurement Collection

4.1.1 Triangulation

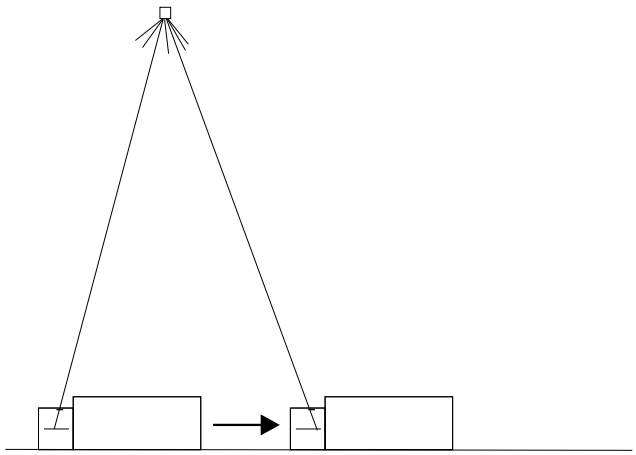

Figure 16: A courier moving to two positions to estimate the LED location.

One basic measurement that can be made involves triangulating from two different courier locations to measure the relative position of an OHM. Each measurement from the OCS can be thought of as a line traveling through the LED, OCS pinhole (lens), and the PSD at the spot reported by the sensor. If the lines are drawn in the fixed courier base frame (c0), they should intersect at the LED.

The triangulation procedure consists of five steps:

1. Move the courier to at least two positions on the platen. Save the actuated values of the courier joints as well as the OCS output.
2. For each position measured, transform the nominal lens position and OCS spot position to the $c0$ frame using Eq. 3.3 and Eq. 3.4.

3. Generate the equation of a line in the $c0$ frame that travels through the OCS spot position and nominal lens position.

4. Finally run a least-squares algorithm to find the point in the $c0$ frame that minimizes the squared-distance to every line.

5. This point is our estimate for the LED in the $c0$ frame.

An example of how to implement this in matlab is included in the appendix.

4.1.2 Data Collection Procedure

Many sets of system configuration measurements, each containing the actuated joint values and corresponding OCS outputs will be collected.

With calibration equipment already built into the courier and OHM, the process of collecting measurements is simplified. The calibration equipment does not need to be reassembled or disassembled for each calibration, thereby saving time. And, furthermore, as measurements can be taken automatically, the process is not labor-intensive.

The built-in calibration equipment thus enables large quantities of data to be collected over a wide range of configurations. This is important in order to minimize the effect that random variation in any one measurement has on the recovered unknown parameters. Reducing this random variation makes the recovered model parameters less sensitive to noise, and therefore more reflective of the real system's parameters.

The data collection procedure is described

1. Extend prismatic joint of the OHM fully.

2. Rotate the revolute joint of the OHM to $0°$.

3. Triangulate the LED using the procedure shown in section 4.1.1.

4. Estimate the current location of the LED using the initial triangulated position, and the current actuated OHM values.

5. Using the estimated LED location, predict where the courier can move on the platen and obtain valid sensor readings from the OCS. This is a $38°$ cone starting from LED diode and extending to the top of the OCS.

6. The largest 10×10 square grid of points centered below the LED in this 38 degree cone is generated.

7. Move the courier to each grid point. At each point the measured joint variables of the OHM and courier are recorded along with the OCS's output.

8. Rotate the OHM 40°

9. Steps 4->8 are repeated until the OHM rotates 360°

10. Retract the OHM's prismatic joint 10 mm.

11. Steps 4->10 are repeated until the OHM's prismatic joint is completely retracted.

The values selected for the relative motions of the OHM as well as the number of grid points were experimentally found to position the courier and OHM at many different configurations. Different numbers could be selected, however for the reasons outlined at the start of this section it is important to select numbers that result in collecting many measurements spread over the courier/OHM configuration space.

4.2 Identification

In this section, the measurements from the data collection procedure and model developed in section 3 are used to recover the parameters in the courier/OHM pair.

To recover these parameters, it is assumed that the model's OCS output closely matches the measurement's recorded OCS output if both systems are excited with identical inputs. For this to be true, the model must accurately reflect the measured system. Note that the model predicted OCS output and the measurement's OCS output will never exactly match due to noise in the collected measurements.

The assumption that the model and real system act very similar given identical inputs provides a way of checking how good a set of parameters fit the collected measurements. Recall, each measurement recorded from the data collection procedure contains the variable inputs for the model (cd_1,cd_2,ct_3,mt_1,md_2) and the x,y output from the OCS. To determine how well a set of parameters match the measurements observed, each measurement's variable inputs are injected into the model along with the parameters to be checked. The current measurements output is then compared against the model output. the parameters are assumed to be a good fit, if the outputs closely match over the measurements.

A metric, *spotError*, is defined, to quantify how good a set of parameters fit the measurements collected.

1. For each measurement, the observed and model predicted OCS spot positions are subtracted to form x and y error values.

2. The error values for all the measurements are combined into a 2nx1 vector, where n is the number of measurements collected.

3. The smaller the norm of this vector, the better the fit.

At this point recovering the parameters has been reduced to a nonlinear optimization problem where the goal is to minimize *spotError*. We use a Matlab function, *lsqnonlin*, which varies the thirteen unknown model parameters (Table 5) in order to minimize the *spotError* metric. This algorithm, *lsqnonlin* is a subspace trust region method and is based on the interior-reflective Newton method [9]. The basic idea of trust region methods are to approximate the high dimensional function to be minimized with a simpler function. This simpler function reasonably reflects the high dimensional function in a neighborhood around the current best point. A trial point is calculated by minimizing the simpler function this neighborhood (or trust region). The trial point is then input into the high dimensional function. If the trial point is an improvement over the previous best point, then the trial point becomes the best point. If the trial point is not an improvement over the current point, then the trust region is shrunk and a new minimized point is calculated. This process is repeated, until a new minimum cannot be found, or the *spotError* is smaller than a tolerance threshold.[10]

Just because the algorithm terminates, does not necessarily mean that the parameters from the measured system were recovered. Several problems can occur that prevent the algorithm from finding the measured system's parameters. If the initial starting point is not close enough to the measured system the algorithm may get stuck in a local minima. A unique set of parameters might not be found because not enough measurements were collected, or they were collected in a way that the measurements don't provide enough information. Some of these concerns can be alleviated by looking at the jacobian of the cost function. This is done in section **??**.

To summarize, a data collection procedure was described to collect many measurements over the courier/OHM configuration space. In addition, a technique for recovering the measured systems parameters was developed using the measurements, model and a nonlinear optimization algorithm.

5 Simulation Results

This chapter discusses simulated results which shows 1) How closely the calibration procedure recovers each unknown parameter; 2) The pose error for a typical calibrated courier/OHM pair in each dimension; 3) An estimate of how well the calibration procedure works in general using a montecarlo simulation; 4) How sensitive the calibration procedure is to each parameter.

The measured system was simulated in matlab. The model of the measured system is identical to the one described at the end of section **??**. In order to more accurately simulate the real courier/OHM pair, noise from each sensor and the resolution of each actuator (see section **??**) is added to the measurements.

Simulating the measured system has several advantages over collecting measurements from a real courier/OHM pair. In the simulated system, the courier/OHM parameters used to generate the OCS outputs are known. This allows one to compare each parameter recovered in the calibration procedure against the corresponding measured system parameters. This lets one confirm that the measured systems parameters are correctly determined. Directly measuring these parameters on a real system is very difficult, if not impossible.

Using a simulated measured system makes it easier to compare how well the calibrated system predicts the measured system's end effector pose . This is because the measured system's end effectors are always known precisely. Comparing the calibration predicted end effector poses vs the measured systems end effector poses, over many configurations, gives one an idea of how well the calibrated system predicts the measured system. Measuring the physical systems pose, particularly over many different configurations is difficult and time consuming.

Yet another advantage of simulating the measured system is the ability to model specific systems which are impossible to create in a real courier/OHM pair. For example the tilt of the PSD inside the OCS housing can be varied while leaving all of the other parameters at their nominal values. By inspecting how well the calibration procedure works on these specific systems one can gain some insight into the importance of recovering each parameter.

Simulating the measured system does not come without drawbacks. The most significant drawback to simulating the measured system is the risk that the modeled system does not behave like a real courier/OHM pair. If this is the case, not only are the simulation results unreliable, but the entire calibration procedure may not work. Therefore, it is necessary to verify the calibration procedure on a real courier/OHM pair. Unfortunately, a manufacturing

problem with the couriers prevents this from being done at this time so only simulated results are shown.

5.1 Simulation Setup

For each simulation, the measured system is constructed by selecting a value for each parameter shown in Table 5. The value of each parameter is selected randomly from a uniform distribution over it's tolerance range. The simulated OHM base frame is placed $150mm \pm 5mm$ above the courier work surface when fully extended. The OHM was placed at this height so the end effector was near the courier work surface when fully extended. The position of the OHM on the platen was arbitrarily selected to be $50mm \mp 5mm$, $50mm \mp 5mm$ as the position has no effect on the calibration procedure.

5.2 Typical results

Typical results of the calibration procedure are shown in Table 6. This table shows how close each recovered parameter is to the corresponding measured systems parameter. This comparison is useful to confirm that the calibration procedure closely recovered the measured systems parameters. It does not, however, provide any direct insight into how well the end effectors can be predicted using the calibrated parameters.

Unknown Params	True value	Calibration recovered value	diff
$T^{c0}_{m0,x}$	$1.498 \times 10^{02} mm$	$1.498 \times 10^{02} mm$	$-2.784 \times 10^{-04} mm$
$T^{c0}_{m0,y}$	$6.507mm$	$6.507mm$	$-2.676 \times 10^{-4} mm$
$T^{c0}_{m0,z}$	$3.259mm$	$3.260mm$	$-9.682 \times 10^{-4} mm$
T^{c0}_{m0}, γ	$-0.4937°$	$-.4937°$	$-5.757° \times 10^{-5}$
T^{c0}_{m0}, ψ	$-90.023°$	$-9.023e+01°$	$2.753° \times 10^{-4}$
T^{c0}_{m0}, ϕ	$4.377° \times 10^{-2}$	$4.378° \times 10^{-2}$	$-1.184° \times 10^{-5}$
$ma2$	$50.24mm$	$50.24mm$	$-7.307 \times 10^{-5} mm$
θ_{c4}	$-.1223°$	$-.1223°$	$4.842e-5°$
θ_{c5}	$-90.51e°$	$-90.51°$	$1.951° \times 10^{-4}$
θ_{c6}	$3.039° \times 10^{-2}$	$3.034° \times 10^{-2}$	$4.656° \times 10^{-5}$
$Lens^{c3}_{x}$	$4.646 \times 10^{-2} mm$	$4.651 \times 10^{-2} mm$	$-4.650 \times 10^{-5} mm$
$Lens^{c3}_{y}$	$-1.886 \times 10^{-2} mm$	$-1.874 \times 10^{-2} mm$	$-1.232 \times 10^{-04} mm$
$Lens^{c3}_{z}$	$14.99mm$	$14.99mm$	$-5.628 \times 10^{-5} mm$

Table 6: The unknown parameters we recovered from a typical system.

5.3 Typical pose accuracy

A more informative comparison is made by calculating, over many configurations, the pose error between the calibration predicted and measured systems end effectors. When doing this comparison the sensor noise and actuator resolutions are excluded from the measured system. If they were included them it would confound the repeatability of the system with how well the calibration procedure predicts the measured systems end effector.

Without noise, there exists no position or orientation error between the predicted and measured courier end effector frames.This is due to the definition of the base and end effector courier frames (see section 3.1). Defining the courier frames in this way, means all of the error between the measured system and calibration predicted system occurs between the $c0$ frame and the OHM end effector frame, $m2$. For this reason only a comparison between the measured systems $m2$ frame and the calibration predicted $m2$ frame is made.

To estimate the average pose accuracy, 1000 random configurations are selected from the OHM/courier configuration space. For each configuration, the transform relating the measured systems $m2$ frame with respect to the the calibration predicted $m2$ frame is calculated using the Euler convention (Z,Y,X).

Table 7: Comparisons between the measured system and the calibration predicted OHM end effector frame , using the Euler convention ($Z(\phi)$, $Y(\theta)$, $X(\psi)$).

Direction	Uncalibrated Error	Calibrated Error
x	$1.740mm$	$4.865 \times 10^{-4}mm$
y	$1.769mm$	$4.891 \times 10^{-4}mm$
z	$0.32mm$	$2.793 \times 10^{-4}mm$
Orientation	Uncalibrated Error	Calibrated Error
θ	$4.479^\circ \times 10^{-2}$	$.002^\circ \times 10^{-5}$
ψ	$9.809^\circ \times 10^{-3}$	$.002^\circ \times 10^{-5}$
ϕ	$2.5^\circ \times 10^{-2}$	$7.88^\circ \times 10^{-6}$

Table 7: Typical results of the average pose errors

5.4 MonteCarlo Simulation

In order to estimate how well the proposed calibration procedure works on average A Monte Carlo simulation, consisting of 50 trials, was executed in order to estimate how well the proposed calibration procedure works on average. The results are shown in Table 8.

Direction	Error
x	$3.23 \times 10^{-5} mm$
y	$3.54 \times 10^{-5} mm$
z	$1.419 \times 10^{-4} mm$
Orientation	Error
θ	
ψ	
ϕ	

Table 8: The average pose error over 50 trial simulations.

5.5 Sensitivity Analysis

The pose errors between the measured system and the calibration predicted end effector positions may be more sensitive to particular parameters. In addition, how well the calibration procedure generally recovers a parameter affects the pose error. These dominate parameters could be pre-calibrated to improve the pose accuracy. Two ways of determining these dominate parameters are tried. The first one involves running the calibration procedure on specific systems. The second way involves examining the jacobian of the solution at the best fit point.

5.5.1 Numerical Sensitivity Analysis

Each parameter was varied over its tolerance range while keeping the remaining parameters at their nominal values. The calibration procedure was run for each of these cases.

Reporting each pose error component (x,y,z,γ,ψ, and ϕ), as each model parameter varies over its tolerance range, results in an incomprehensible amount of data. A better alternative is to create metrics for the position and orientation error. The position metric, called $positionPoseError$, is defined as the norm of the position error between the predicted and actual OHM end effector frames. The orientation metric, called $orientPoseError$, is defined as the norm of the orientation error between the predicted and actual OHM end effector frames.

Each parameter was varied over it's tolerance range, while keeping the remaining parameters at their nominal values. The calibration procedure for each case was run. The $positionPoseError$ and $orientPoseError$ are shown for the $ma2$ parameter. The remaining figures are shown in the appendix because the $m2$ graphs are representative of the other parameter's graphs. These graphs show that the calibration procedure is relatively stable

over every parameters tolerance range.

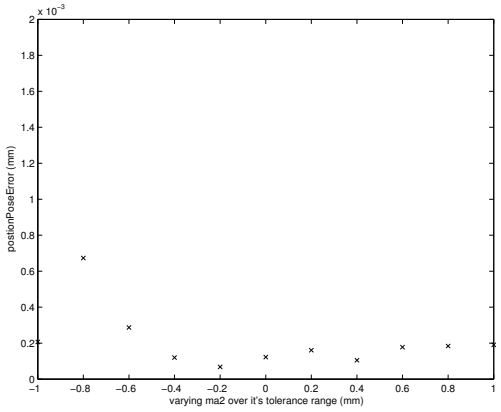

(a)

5.5.2 Jacobian Analysis

The numerical estimate of the jacobian at the minimized point also provides some insight into how distinct each parameter is at this point. The numerical estimate of the jacobian returned by $lsqnonlin$ is an m by n matrix, where m is the number of measurements collected and n is the number of parameters (13 in our case). Singular value decomposition (SVD) is used determine the singular values and singular vectors of the jacobian. Examining the right singular vectors that correspond to the smallest singular values provides an insight into what parameters share the most redundancy. The three smallest singular vectors in the solutions this calibration procedure produces show the position of the pinhole is somewhat redundant with the position of the OHM's base frame. This suggests that an improvement in calibrating the transform between the courier and OHM base frames could be made if the position of the lens relative to the PSD was pre-calibrated.

6 Conclusion

In this report, the physical components related to calibrating minifactory was analyzed to determine which effects were relevent to calibrating the courier/OHM pair. A model of these effects on the output of the OCS was constructed. Furthermore, a data collection algorithm was created to automatically collect courier/OHM measurements over a wide range

of configurations. The measurements were then used with the model to recover the unknown relationship between the courier and OHM. Finally a simulation of the courier/OHM pair was calibrated. Typical results from the simulation showed the euclidian distance between the predicted pose, and actual pose was less than 1um.

7 Future Work

The immediate future goal is to measure the calibration procedures performance on a real courier/OHM pair. To do this the data collection procedure needs to be converted and ran on the courier and OHM. A technique for measuring how well the real system is calibrated also needs to be developed.

Another goal is to relate the end effector frames defined here to the working end effectors. This requires a techique to be developed to measure the OHM's working end effector from the recovered kinematics of the OHM. Additionally a way of measuring from the courier's end effector frame ($c3$) to the OHM needs to be developed.

Other goals include modeling the OCS as a more complex lens that includes radial distortion. This might be done by adding parameters for the projection matrix of the lens, and radial distortion parameters [11].

References

[1] M. S. Laboratory, "http://www-2.cs.cmu.edu/afs/cs/project/msl/www/minifactory/aaa.html." World Wide Web.

[2] M. L. Chen, "Visually guided coordination for distributed precision assembly," Master's thesis, Carnegie Mellon University, December 1999.

[3] B. A. Sawyer, "Linear magnetic drive system." U. S. Patent 3,735,231, May 22 1973.

[4] A. E. Quaid, *A Planar Robot for High-Performance Manipulation.* PhD thesis, Carnegie Mellon University, 2000.

[5] Z. J. Butler, A. A. Rizzi, and R. L. Hollis, "Integrated precision 3-DOF position sensor for planar linear motors," in *Proc. IEEE Int'l. Conf. on Robotics and Automation*, (Lueven, Belgium), May 1998.

[6] W.-C. Ma, "Precision Optical Coordination Sensor for Cooperative 2-DOF Robots," Master's thesis, Carnegie Mellon University, 1998.

[7] W.-C. Ma, A. A. Rizzi, and R. L. Hollis, "Optical coordination sensor for precision cooperating robots," in *IEEE International Conference on Robotics and Automation*, vol. 2, (San Francisco, CA), pp. 1621 – 1626, April 2000.

[8] L. Sciavicco and B. Siciliano, *Modelling and Control of Robot Manipulators.* Springer, 2003.

[9] The Math Works, "http://www.mathworks.com/access/helpdesk/help/toolbox/optim/lsqnonlin.html" World Wide Web.

[10] The Math Works, "http://www.mathworks.com/access/helpdesk/help/toolbox/optim/tutori2d.html." World Wide Web.

[11] J. P. David Forsyth, *Computer Vision A modern approach.* Prentice Hall, 2003.